

# Soft actuators inspired by a muscle-cross-bridge

Zhaowen Shao, Wentao Zhao, Zhaotian Zuo and Jun Li\*

## Abstract

Soft actuators have a high potential for safe human-robot interaction and the creative design of flexible robots. Making soft actuators act like human muscles has been a sustained goal of researchers worldwide. So far, significant progress has been made in flexibility, deformation amplitude, and variable stiffness of soft actuators. However, there are still deficiencies in output force and force retention. Human muscle has ideal force performance, mainly due to muscle cross-bridge structures' motion. Inspired by cross-bridges, this paper proposes a new folding design of soft actuators driven by negative pressure fluid. Meanwhile, we establish a theoretical model to predict such an actuator's output force and displacement under given pressures. Next, five actuators are fabricated using three different materials and evaluated on a test platform. The test results reveal that one generates the maximum pull force of 1125.9N and the maximum push force of 818.2N, and another's full output force reaches 600 times its weight. Finally, demonstrative experiments are conducted extensively, including stretching, contracting, clamping, single-arm power assistance, and underwater movement. They show our actuators' characteristics of a large output force, strong force retention, two-way working, and even generating human-muscle-like explosive force. The valuable properties are lacking in the existing soft actuators.

**Keywords:** soft actuator, muscle-cross-bridge, output force, force retention, two-way locomotion, explosive force

## Introduction

Rigid robots have inherent deficiencies in flexibility and adaptability and thereby struggle to meet the increasing needs of flexible operation. In the past decade, people continuously studied a variety of soft robots composed of flexible materials. They have natural flexibility and adaptability for flexible operations. As power components of soft robots, soft actuators have attracted more and more attention.

There are two kinds of soft actuators in the literature, i.e., electric soft actuators and fluid-driven ones. A typical electric soft actuator is made by shape memory alloy (SMA), dielectric elastomer (DE), or ionic polymer-metal composites (IPMC). SMA actuators<sup>1-4</sup> perform the alloy's phase conversion to stretch in a relatively slow response to heating. DE actuators<sup>5-6</sup> exploit the electrostatic interaction between two electrodes to produce deformation. However, it requires a very high driving voltage and cannot ensure stable deformation.<sup>7</sup> IPMC<sup>8-11</sup> can produce larger deformation but a smaller output force.

Compared with the electric actuators, fluid-driven soft actuators have prominent superiorities in deformation amplitude, response speed, and output force. Therefore, they have been the research focus in recent years. Some researchers use hyperelastic materials such as silica gel to make soft actuators.<sup>12-18</sup> These actuators work via the cumulative deformation caused by the expansion of silica gel material under positive pressure. The maximum output force they can produce is about 1.2 ~ 15.2N and primarily be used to produce large deformation. On the other hand, some studies reinforce soft actuators by adding fibers to silica gel materials.<sup>19-21</sup> The maximum output force of these actuators can be up to 25 ~ 40N. In addition, some soft actuators are made of fiber materials.<sup>22-28</sup> The maximum output force of them is about 45 ~ 320N. Further, to achieve a greater output force, some works use the rigid folding skeleton sealed with a tough impermeable film to form soft actuators.<sup>29-33</sup> As a result, the output force generated can reach 90 ~ 630N.

The fluid-driven soft actuators mentioned above, regardless of material and structure, almost have a common feature, i.e., the output force decreases significantly with the increase of displacement. Therefore, it leads to poor force retention during work. Specifically, their output force is maximal at the initial position and decays rapidly with the increasing displacement under constant pressure. Therefore, it may result in accidental situations such as state instability and damage.

Some studies improve the retention ability of actuators with variable stiffness during work.<sup>34-40</sup> But variable stiffness can only maintain some specific positions statically. At the same time, variable stiffness may restrict the actuator's motion capability and output force.

In summary, substantial progress has been made in promoting the output force of soft actuators, but their force retention is still far from enough. However, soft actuators must have either large output force or strong force retention for some flexible operations.

Human muscles can output a large force at high speed<sup>41</sup> and even explosive force.<sup>42-43</sup> It owes primarily to the work of cross-bridges in muscles.<sup>41</sup> Unfortunately, few soft actuators have both properties. Inspired by muscle cross-bridges, we propose a new soft actuator paradigm with a folding skeleton and a sealed skin in this paper. Sealed by a soft film, such a soft actuator, it can be driven by negative pressure air or liquid and work in two ways. Furthermore, its output force increases significantly with the increase of displacement and can reach infinity in theory.

The main contributions of this work are as follows. (1) We propose a novel two-way stretching soft actuator structure inspired by muscle cross-bridges. The negative-pressure fluid-driven actuator has strong force retention and large output force simultaneously. Additionally, it can produce explosive force as human muscles do. We fabricate five actuators with a patched, 3D printed, or machined skeleton. The test results reveal that one generates the maximum pull force of 1125.9N and the maximum push force of 818.2N, and another's full output force reaches 600 times its weight.

(2) We conduct several innovative demonstrations of the actuators, including stretching, contracting, clamping, single-arm power assistance, and underwater movement. They show our actuators' characteristics of a large output force, strong force retention, two-way working, and even generating explosive force as human muscles do. The valuable properties are lacking in the existing soft actuators. In addition, the demonstrations indicate the excellent application potential of our soft actuators.

The rest of this paper is organized as follows. First, the folding skeleton is presented in Section II, and the soft actuator scheme is designed and analyzed in Section III. Then, we fabricate five actuators and evaluate their performances in Section IV and V, respectively. Next, Section VI demonstrates several application scenarios. Finally, Section VII concludes the work.

### Muscle Cross-Bridge-Inspired Folding Structure

As illustrated in Figure 1a, a whole muscle is composed of many muscle filaments in parallel.<sup>41</sup> Each muscle filament includes numerous sarcomeres in series, and each sarcomere comprises several parallel cross-bridges. A cross-bridge consists of the attachment points of myosin and myosin heads on actin filaments,<sup>44</sup> as shown in Figure 1b. By the myofilament sliding theory, a muscle retracts through the motion of a large number of cross-bridges.

A cross-bridge is a fundamental component of muscle contraction, and its energy comes from ATP hydrolysis.<sup>41</sup> By the myofilament sliding theory, a myosin head and actin are bound reversibly via molecular force. The myosin head bends with the energy of ATP hydrolysis to drag the actin to move. Under the synergy of multiple sets of symmetrically arranged myosin heads in the cross-bridge, the actin on both sides slides smoothly. It makes the two Z disks at the ends of a sarcomere approach each other and finally shortens the length of the cross-bridge and the sarcomere to generate contraction force.

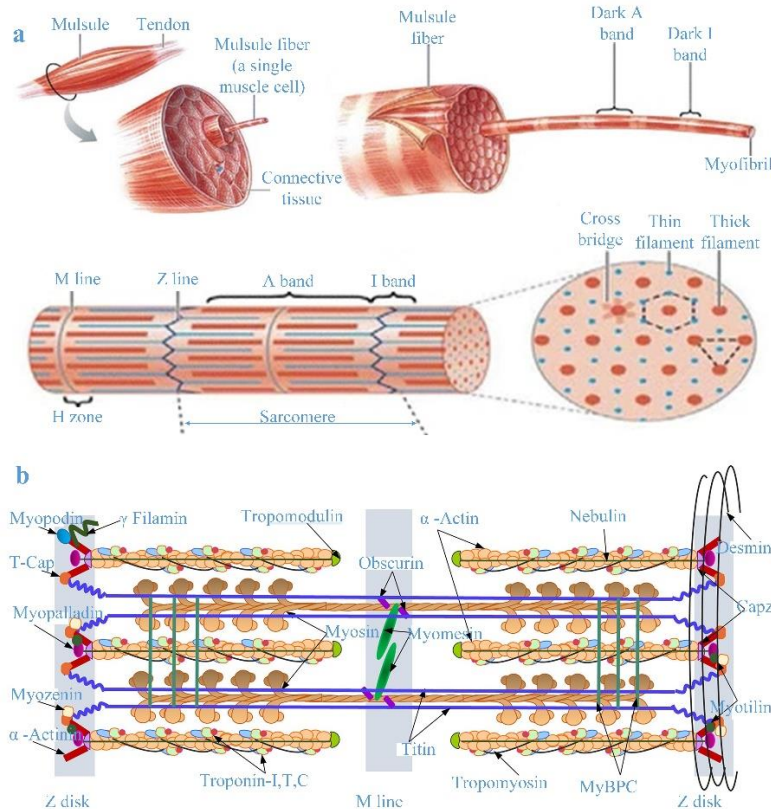


**FIG. 1.** Biological structure of a muscle. (a) Basic composition of a muscle.<sup>41</sup> (b) Cross-bridges in a sarcomere.<sup>44</sup>

We present a cross-bridge-inspired folding structure, as shown in Figure 2a. It uses vertical and horizontal plates to replace myosin heads and actins. Two adjacent plates are connected by a hinge or soft material. The rotation of a vertical plate can drive the sliding of the horizontal plate. Therefore, we layout multiple vertical plates symmetrically to imitate the motion of a cross-bridge. The synergy of the plates enhances the movement effect.

To drive the structure using negative pressure, we seal it with a soft film to form an airtight soft actuator, as shown in Figure 2b. The initial state of this actuator and its load under negative pressure fluid is illustrated in Figure 2b.

Under negative pressure, the actuator can work in two ways, i.e., shrinking and stretching. They depend on the actuator's initial state that is decided by the angle between the vertical and horizontal plates. The actuator's stretching generating a push force and shrinking producing a pull force is shown in Figures 2c, d, respectively.

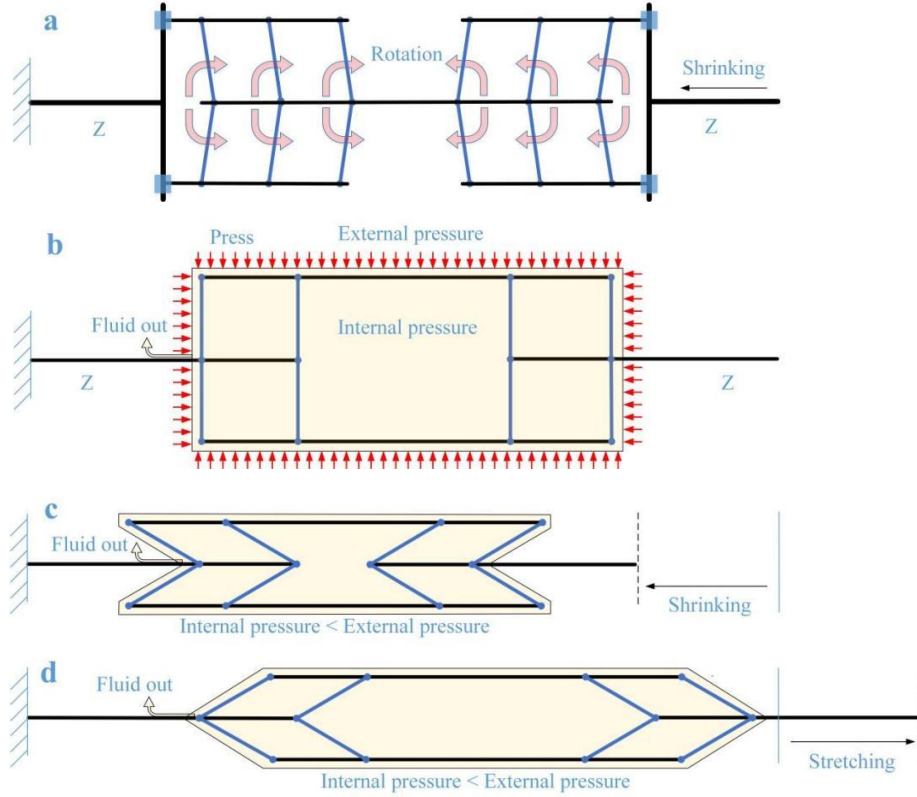


**FIG. 2.** Evolution of cross-bridge-inspired folding structures. (a) Initial configuration. (b) A soft actuator in stretching and its load under negative pressure fluid. (c) The soft actuator in shrinking.

### Design and Mechanical Analysis of Actuator

The initial 3D folding structure is illustrated in Figure 3a. When an actuator of this structure works under negative pressure, the soft film greatly concaves to the inside. As a result, it significantly reduces the output force of the actuator. To minimize such a negative impact, we add side support like butt hinges to the structure, as shown in Figure 3b.

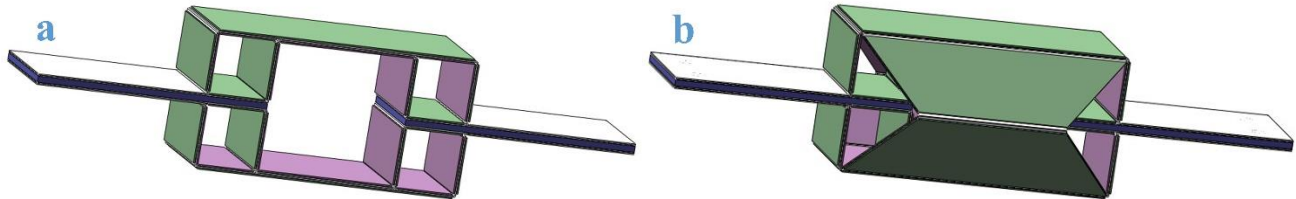


**FIG. 3.** 3D cross-bridge-inspired structures. (a) Initial configuration, and (b) Improved configuration with a side support.

The forces on an actuator with the improved skeleton driven by negative pressure are shown in Figure 4a-c, including  $F_{N2}$  and  $F_{N2r}$  on the side support,  $F_{N1}$ ,  $F_{N2r}$ ,  $F_{N3}$ ,  $F_{N4}$ , and  $F_A$  on the mainframe when shrinking and stretching.  $L_1$ ,  $L_2$ , and  $L_4$  represent the length of each vertical and horizontal plate, respectively. Symbol  $h$  represents the width of each vertical plate and horizontal plate of the skeleton, and  $L_3$  is the width of the side supporting structure. Additionally,  $d_0$  denotes the center distance of two adjacent hinges on both sides of the Z plate, and  $L_0$  is the distance between the outer edge of the upper plate and the axis of the adjacent hinge.

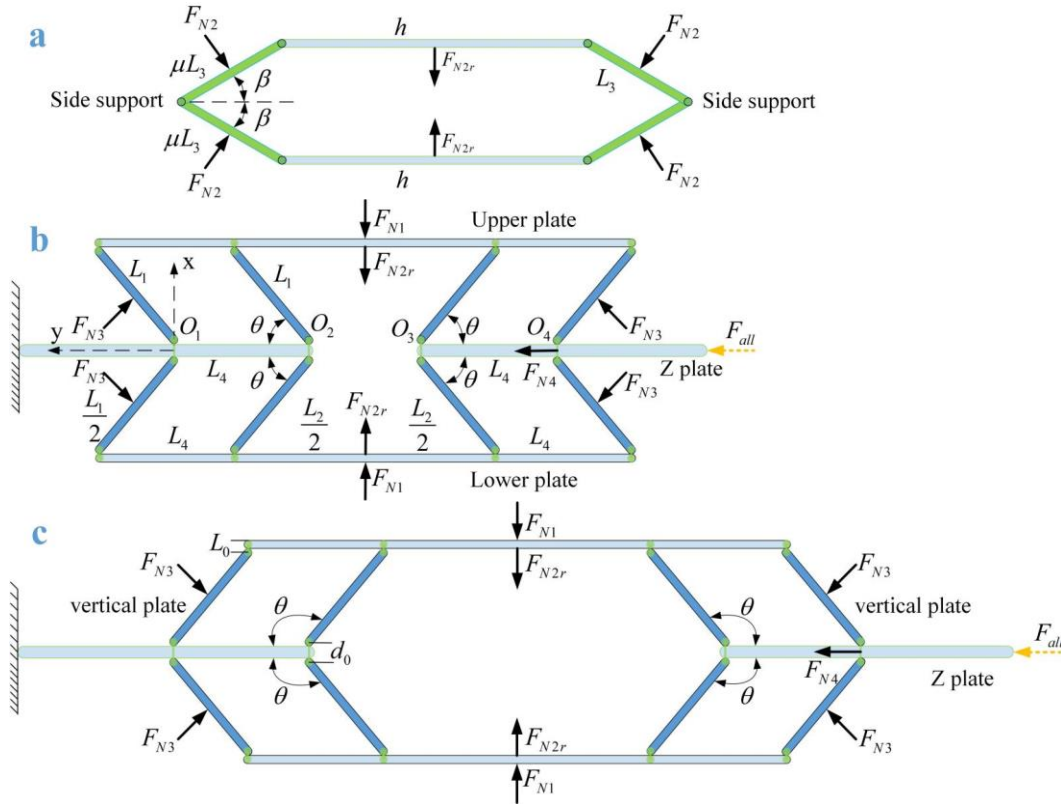


**FIG. 4.** Force analysis of the actuator. (a) Force on the side support. (b) Force on the mainframe when shrinking. (c) Force on the mainframe when stretching.

Assume that the skeleton is rigid and the soft film can be well sealed and the well-sealed soft film's deformation has a negligible effect on the skeleton. Then, during the actuator works, the stress and movement of the skeleton are analyzed as follows:

We first calculate the equivalent concentrated forces on every plate on the skeleton. They are caused by pressure differences between the inside and outside of the actuator. The equivalent concentrated force of the uniformly distributed load on different plates on the skeleton is given by,

$$F_{Ni} = pS_{Ni}, i = 1, 2, 3, \text{ or } 4 \quad (1)$$

where  $S_{N1}$  is the area of an upper plate or lower plate,  $S_{N2}$  is the area of a single plate on the side support,  $S_{N3}$  is the area of a vertical plate,  $S_{N4}$  is the equivalent area of the uniformly distributed load on the single Z plate.  $F_{N1}$ ,  $F_{N2}$ ,  $F_{N3}$ , and  $F_{N4}$  are the equivalent concentrated forces of the uniformly distributed loads on the above plates, as shown in Figure 4.

According to Figure 4a, we convert  $F_{N2}$  on the side into its equivalent concentrated force  $F_{N2r}$  on the mainframe as follows,

$$F_{N2r} = F_{N2} \frac{\mu \sin^2 \beta}{\cos \beta} \quad (2)$$

In Eq. (2),  $\mu$  is the coefficient of the arm of force  $F_{N2r}$  in the above conversion, and its value is determined by the size of the side supporting structure, as shown in Table 1.  $\beta$  is half of the angle between two adjacent side supporting plates, as shown in Figure 4a.  $\theta$  is the angle between the vertical plate and the Z plate, as shown in Figures 4b, c. The relationship between angles  $\theta$  and  $\beta$  can be denoted by,

$$\beta = \arcsin \frac{d_0 + 2L_0 + 2L_1 \sin \theta}{2L_3} \quad (3)$$

Therefore, the total equivalent force on either the upper or lower plate on the skeleton is,

$$F_N = F_{N1} + F_{N2r} \quad (4)$$

Assume that the direction of the output force is positive when the actuator folds. Then, according to the force analysis shown in Figures 4b and 4c, force  $F_t$  generated by the unilateral skeleton can be calculated by,

$$F_t = \frac{\frac{1}{2}F_N \cos \theta - \frac{1}{2}F_{N3}}{\sin \theta} + F_{N3} \sin \theta \quad (5)$$

Thus, we have the total force  $F_{all}$  generated by the pressure difference between the inner and outer sides of the skeleton,

$$F_{all} = 2F_t + F_{N4} \quad (6)$$

Further,

$$\begin{aligned}
F_{all} &= \frac{F_N \cos \theta - F_{N3}}{\sin \theta} + 2F_{N3} \sin \theta + F_{N4} \\
&= p \left( \frac{\left( S_{N1} + S_{N2} \frac{\mu - \sin^2 \beta}{\cos \beta} \right) \cos \theta - S_{N3}}{\sin \theta} + 2S_{N3} \sin \theta + S_{N4} \right)
\end{aligned} \tag{7}$$

During the operation of the actuator, the distance between endpoints  $O_1$  and  $O_4$  on Z plates on the left and right sides of the skeleton is,

$$D = L_2 + 2L_4 - 2L_1 \cos \theta \tag{8}$$

We consider the initial state of the actuator is when the vertical plate is perpendicular to the horizontal plate, or  $\theta = 90^\circ$ . Assume that the direction of the displacement  $S$  is positive when the actuator folds. The displacement  $S$  of the actuator can be expressed as,

$$S = (L_2 + 2L_4) - D \tag{9}$$

Or,

$$S = 2L_1 \cos \theta \tag{10}$$

By Equation (7), the output force of the actuator has a linear relationship with the pressure difference  $p$  between its inner and outer sides. In contrast, it has a nonlinear relationship with angle  $\theta$ . As the actuator shrinks, the angle  $\theta$  gradually decreases while the output force gradually increases. When the actuator shrinks to the limit position,  $\theta$  approaches zero and the output force of the actuator tends to infinity. Similarly, when the actuator is in the extended state, the angle  $\theta$  gradually increases while the output force gradually increases, and its maximum output force tends to infinity.

### Fabrication of Actuator Prototypes

Five actuators of different properties are fabricated. Each has a rigid skeleton supporting the actuator and conducting force output. The patched, machined, or 3D printed skeleton is sealed by an airtight soft film with good toughness to form a sealed cavity.

#### *Patched Actuator*

The fabrication process of the actuator with a patched skeleton is shown in Figure 5. We use a 0.5mm thick white canvas as the soft substrate.

First, we paste several 0.5mm thick PET patches and 0.6mm thick carbon fiber patches onto the specific positions of the canvas' two sides using glue and then get a combination through cutting, folding, pasting, etc., as shown in Figure 5a.

Next, we obtain the skeleton through subsequent operations, as shown in Figure 5b.

Finally, the skeleton is sealed with a 0.1 mm thick TPU film to form an actuator, shown in Figure 5c.

The resultant actuator is illustrated in Figure 6a. The weight of this actuator is 76.5g, and its basic dimension parameters are given in Table 1.

#### *Machined Actuator*

Considering that the patched actuator's fabrication process is too cumbersome and overall rigidity is insufficient, we use aluminum alloy to make the skeleton. Specifically, we machine the individual aluminum alloy plates and assemble them into a skeleton. Then, we seal the skeleton with a 0.1 mm thick TPU film and obtain an actuator shown in Figure 6b. Its weight is 462g, and its dimensional parameters are listed in Table 1 as well.

#### *3D Printed Actuator*

To reduce the fabrication cost, we adopt 3D printing to make the skeleton. This skeleton is assembled from 3D printed plates with elastic beams. The size and stiffness of the skeleton are adjustable by altering the size and material of the elastic beam. It results in actuators of different performances.

First, we use a 3D printer to print the skeleton plates and a laser cutting machine to cut carbon-fiber-plate and PET sheets to obtain elastic beams. Second, we assemble the resultant parts to make up three skeletons and seal each with a 0.1 mm thick TPU film to form three actuators, as shown in Figure 6. The weight of the actuators with a carbon-fiber-plate beam and a PET beam is 242g and 240g, respectively. The sizes of the actuators with a 3D printed skeleton are the same as the actuator with a machined skeleton. Finally, to reflect the influence of the side support on the actuator's performance, we fabricate an actuator without side supporting structures, as shown in Figure 6e. Its size is the same as the actuator with side support.

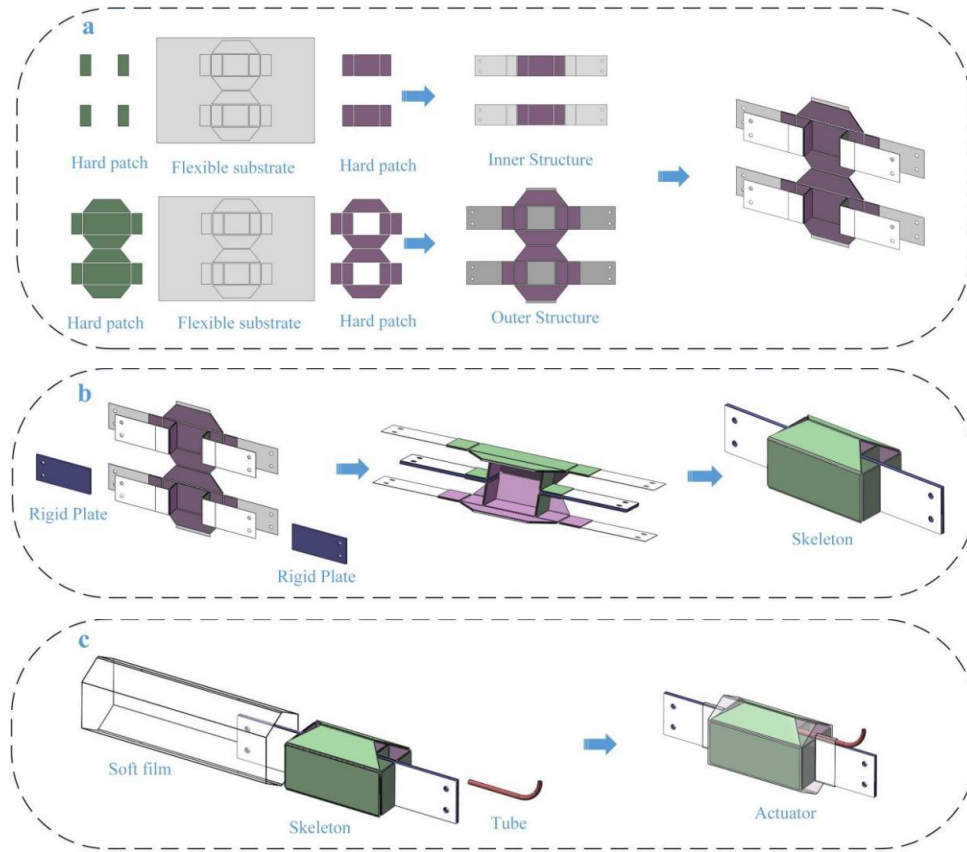


**FIG. 5.** Fabrication process of the actuator with a patched skeleton. **(a)** Paste the hard patch on the flexible substrate. **(b)** Combine the rigid patch and the soft substrate into a skeleton. **(c)** Seal the skeleton with a soft film to obtain an actuator.

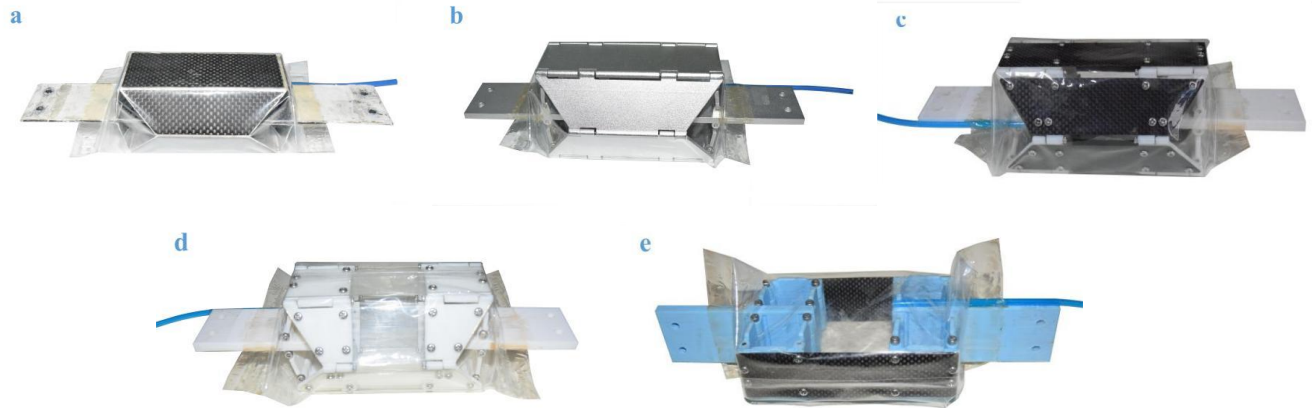


**FIG. 6.** Actuators. **(a)** Actuator with a patched skeleton. **(b)** Actuator with a machined skeleton. **(c)** Carbon-fiber-beamed actuator. **(d)** PET-beamed actuator. **(e)** Actuator without a side support.

Table 1 Basic parameters of different actuators

Actuators	Length(mm)							Coeffi- cient $\mu$	Area(mm <sup>2</sup> )			
	$L_1$	$L_2$	$L_3$	$L_4$	$d_0$	$L_0$	H		$S_{N1}$	$S_{N2}$	$S_{N3}$	$S_{N4}$
Patched skeleton	22	52	27	22	3	0	42	0.55	4032	2025	924	0
Machined skeleton	22	54	40	32	14	6	42	0.54	5875	3844	630	882
3D printed skeleton	22	54	40	32	14	6	42	0.54	5875	3844	630	882

## Performance Test

### Experimental Setup

We design a test platform to test the soft actuators and evaluate their performance, as shown in Figure 7. One end of an actuator is connected to a tension-compression sensor to measure the actuator's output force. Another end links to an electric push rod to control the actuator's stretching measured by a displacement sensor. The pressure of an actuator is derived from a vacuum pump with an air-vacuum proportional valve and a solenoid valve.

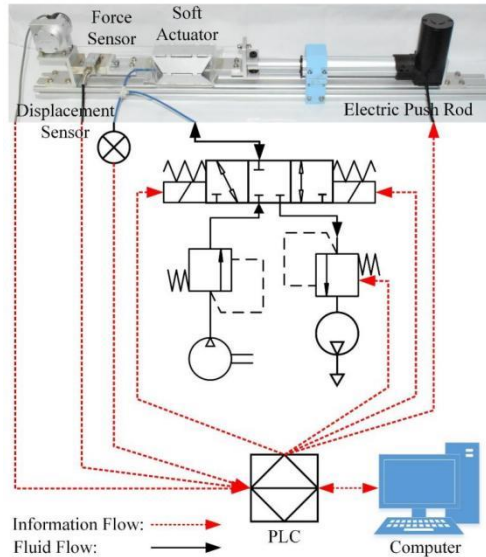


FIG. 7. Test platform.

The main components of the test platform include a pull rope displacement sensor MPS-S-1000mm from Shenzhen Milont Technology Co., LTD, a tension-compression sensor LLBLS-I from Shanghai Longlvdianzi Technology Co., Ltd, a vacuum manometer ZSE30AF-01-E, an air-vacuum proportional valve ITV0090-3BL, solenoid valve VEX3121-025DZ-FN, and pressure reducing valve AW20-01BG-A from SMC, a vacuum pump 550D, from Taizhou Fujiwara Tools Co., Ltd.

### Test Results and Analysis

The test results of the actuators are shown in Figure 8, and the statistics of the test are listed in Tables 2-5, respectively.

As shown in Figures 8a, c, e, the output force of actuator with a patched skeleton, the actuator with a machined skeleton and the PET-beamed actuator with a 3D printed skeleton is slightly less than the force predicted by their theoretical model. The reason may be that the soft films are trapped into the skeleton due to pressure difference and offsets part of the output force of the skeletons. As shown in Figure 8g, the output force of carbon-fiber-beamed actuator with a 3D printed skeleton is slightly less than the predicted value obtained by the theoretical model in the first half of the motion process. It is mainly affected by the soft film. The output force of the second half of the motion process is slightly greater than the theoretical model's predicted value due to the small bending of the elastic beam to the inside.

As shown in Figures 8a, c, e, and g, the overall shape of the output force curves of each actuator is almost consistent with their theoretical curves. Under constant pressure, the output force of the actuators increases gradually with the arising displacement, and the growth is faster and faster. By the experimental results, as the pressure difference increases, the deviation between the output force and the model predicted value gradually increases with the film shrinking towards the skeleton inside. In addition, we observed an approximately linear relationship between the output force of the actuator and the pressure at a given displacement, as shown in Figures 8b, d, f, and h. Again, it is consistent with the prediction of the theoretical model established in Section III.

The flexible substrate between two adjacent hard patches acts as a rotating shaft in the patched skeleton. Nevertheless, the rotating shaft can remain stable only when the flexible substrate is under tension. Therefore, the actuator with a patched skeleton can only work effectively in contraction. In the experiment, the actuator can produce a pull force of 450N under pressure 45kPa, equivalent to 600 times the actuator's gravity. Meanwhile, the skeleton has undergone a large deformation, and continuing to increase the pressure leads to damage to the actuator.

The actuator with a machined metal skeleton can bear the force in all directions and work during elongation and contraction. When the pressure is 48.5kPa, the actuator can generate a pull force of 1125.9N, 248.5 times its gravity, and a thrust force of 818.2N, 180.6 times its gravity, as given in Table 3. We do not further test its mechanical properties provided higher pressure, considering the experimental safety. Both Equation (7) and Figure 8 show an approximately linear

relationship between the actuator's output force and the given pressure. The maximum vacuum pressure in the air can reach about -101kPa. Therefore, the tests can only examine about half of the potential of the actuator.

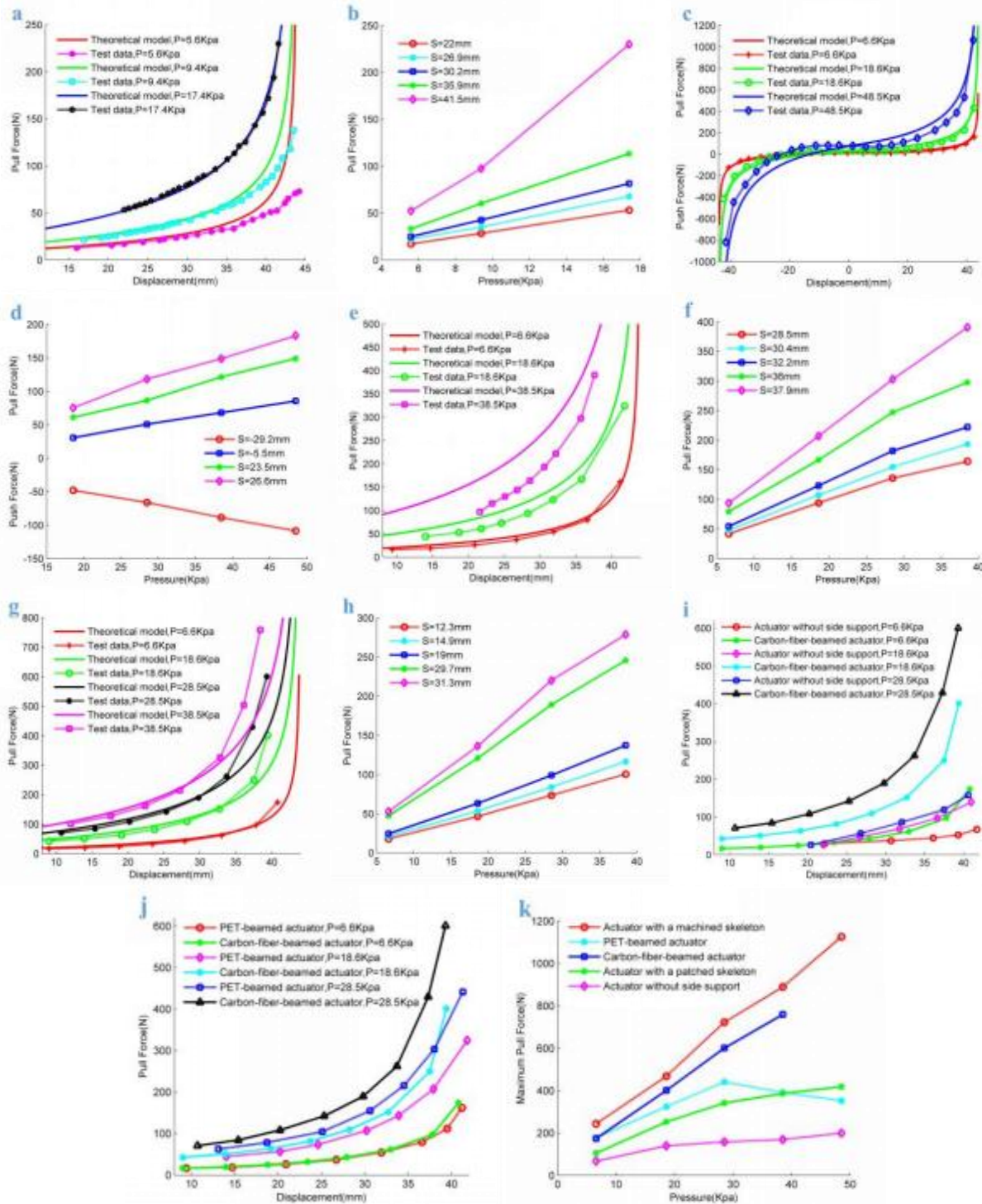


**FIG. 8.** Test results of actuators. (a), (b) Test results of the actuator with a patched skeleton. (c), (d) Test results of the actuator with a machined skeleton. (e), (f) Test results of the PET-beamed actuator with a 3D printed skeleton. (g), (h) Test results of the carbon-fiber-beamed actuator with a 3D printed skeleton. (i) Comparison between the actuator without side supporting structure and the carbon-fiber-beamed actuator with a 3D printed skeleton. (j) Comparison between PET-beamed actuator and carbon-fiber-beamed actuator. (k) Comparison of the maximum output force of different actuators.

Table 2 Summary of the test data of the actuator with a patched skeleton

Test	Pressure (kPa)	Peak force (N)	MAE	MAPE	Maximum absolute error	Data sources
1	5.6	72.9	32.84	79.33	309.96	21
2	9.4	137.9	14.55	35.77	154.84	29
3	17.4	229.8	2.60	3.19	7.69	25

Table 3 Summary of the test data of the actuator with a machined skeleton

Test	Pressure (kPa)	maximum tension force (N)	maximum thrust force (N)	MAE	MAPE	Maximum absolute error	Data sources
1	6.6	243.3	-125.2	11.82	13.82	42.86	62
2	18.6	468.1	-410.1	30.58	37.97	168.86	71
3	28.5	722.5	-409.5	46.50	52.37	144.47	55
4	38.5	889.3	-628.9	67.85	77.14	199.03	50
5	48.5	1125.9	-818.2	86.96	100.01	244.58	44

Table 4 Summary of the test data of the PET-beamed actuator

Test	Pressure (kPa)	Peak force (N)	MAE	MAPE	Maximum absolute error	Data sources
1	6.6	177	6.81	6.91	8.41	19
2	18.6	324.4	29.89	36.14	104.76	15
3	28.5	441	47.40	52.93	128.42	15
4	38.5	390.7	73.34	73.59	86.26	9
5	48.5	352.5	117.67	117.95	130.56	5

Table 5 Summary of the test data of the Carbon-fiber-beamed actuator

Test	Pressure (kPa)	Peak force (N)	MAE	MAPE	Maximum absolute error	Data sources
1	6.6	174	6.32	8.47	30.50	21
2	18.6	400.9	15.33	28.49	118.58	20
3	28.5	600.7	25.39	51.16	186.73	18
4	38.5	759.4	34.67	72.92	264.41	16
5	48.5	##	15.70	19.29	49.45	12

The actuators with a 3D printed skeleton can transmit the force through the elastic beam. Therefore, its mechanical performances depend on the stiffness of the elastic beam to a certain extent. The stiffness of the PET beam is relatively smaller, making it challenging to bear push force in the length direction. Thus, the actuator with a PET-beamed 3D printed skeleton can produce a larger pull force but a relatively smaller push force. By testing, the PET-beamed actuator can reach a maximum pull force of 595.6N, 253.4 times its gravity, but the full thrust generated is only 79N. In contrast, the carbon-fiber beam is stiffer, so the carbon-fiber-beamed actuator with a 3D printed skeleton can cause large pull and push forces. Experimental tests show that it can achieve a maximum pull force of 759.4N, 320.4 times its gravity.

There is a particular gap at each joint of the skeleton in all the actuators mentioned above. It leads to a certain motion redundancy. Under the pressure difference between the inner and outer sides, the actuators can keep the state stable by the mutual restriction between the skeleton components. The experimental results show that increasing the overall stiffness of the skeleton or the motion amplitude of the actuator can improve the structural stability of the actuator. In addition, as the pressure difference between the inner and outer sides increases, the structural stability of the actuator is depressed.

#### Performance Comparison of Different Actuators

To explore the effect of side support on the performance of an actuator, we compare the carbon-fiber-beamed actuator with a 3D printed skeleton and the actuator without side support. As shown in Figure 8i, the output force of the former is significantly greater than that of the latter concerning the same displacement under a certain pressure. Thus, the side support dramatically improves the output force of an actuator. On the other hand, the side support increases the internal restriction in a skeleton and significantly enhances the morphological stability of an actuator.

Similarly, we compared the PET-beamed actuator and the carbon-fiber-beamed actuator to examine the influence of the skeleton's stiffness on the actuator's performance. Both have a 3D-printed skeleton. As shown in Figure 8j, the output force of the former actuator is significantly greater than that of the latter regarding the same displacement under a given pressure.

Note that the PET beam is more apt to dent into the inner of the skeleton than the carbon-fiber-plate beam. It significantly reduces the effective stroke of the PET-beamed actuator. Therefore, the greater the stiffness of the skeleton, the greater the output force of the actuator, and the higher the effective stroke of the actuator, regarding the same displacement and given pressure.

On the other hand, actuators made of different materials have different mechanical properties. For example, as shown in Figure 8k, the greater the skeleton stiffness, the greater the full output force of an actuator under specific pressure.

### **Demonstration of Actuators**

Our soft actuators have some characteristics unexplored before in the existing work. These characteristics include dual-mode work, high force retention, large output force, and some explosiveness. To illustrate them, we design four demonstrations, i.e., push and pull, clamping, single-arm-assisted motion, and motion in water.

Figures 9a-d illustrate two work modes of our actuators, i.e., push and pull in horizontal and vertical directions.

First, the carbon-fiber-beamed actuator with a 3D printed skeleton can push and pull an 8.1kg concrete block horizontally. In the beginning, the actuator in the push mode cannot push the concrete block away. However, once the pressure increases to 45kPa, the actuator shoves the concrete block 4 cm away instantaneously, while it stretches only 2 cm on its own, as shown in Figure 9a and Supplementary Movie S1. It indicates that the actuator can produce explosive force by gradually accumulating strength as human muscles do. Then, when the actuator works in the pull mode, it can pull the concrete block back 2cm under the same pressure, as shown in Figure 9b and Supplementary Movie S2.

Next, the actuator with a machined metal skeleton working in the pull mode can stretch a spring with an elastic coefficient of 3N/mm for 15mm under the pressure of 12kPa, as shown in Figure 9c and Supplementary Movie S3. Besides, the actuator in push mode can break a pencil under the pressure of 25kPa, as shown in Figure 9d and Supplementary Movie S4.

Our actuator with a machined skeleton can produce a huge output force. As demonstrated in Figure 9e and Supplementary Movie S5, the actuator lifts the rebars of 60.5kg instantly for about 7mm without any assistance when the driving pressure is 60kPa. It confirms again that our actuators have some explosive force similar to human muscles'. The actuator's lifting status remains unchanged by keeping the same pressure. It shows that the actuator has excellent force retention.

We design a 3D printed clamping jaw driven by the actuator with a machined metal skeleton. This clamping jaw can clamp the concrete block and keep the clamping when an electric push rod lifts it and the block for 22s, as shown in Figure 9f and Supplementary Movie S6. In the above process, the clamping still holds with no signs of loosening. It shows our actuators' high force retention again.

Also, we design a power-assisted structure for a single-arm using the carbon-fiber-beamed actuator with a 3D printed skeleton, as shown in Figure 9g and Supplementary Movie S7. The actuator tows a wood model's forearm with a Bowden cable. First, the structure bends the forearm to 30° from the original position. Next, we hang a 500ml bottle of water on the wrist when the forearm bends nearly to the horizontal position. Due to the actuator's force retention, the forearm always keeps the status as long as the actuator works.

Our actuators can be driven by liquid under negative pressure as well. For example, we use a large syringe with water to drive the PET-beamed actuator with a 3D printed skeleton. The hydraulic actuator can pull the concrete block to slide 3 cm in water, as shown in Figure 9h and Supplementary Movie S8.

### **Discussion on Our Actuators**

#### *Advantages*

Our muscle-cross-bridge-inspired actuators have many excellent features, as validated and demonstrated by the above experiments. Namely, 1) our actuators can contract and elongate, 2) they can reach tremendous output force, outperforming the existing soft actuators, 3) their output force increases with the growth of displacement, resulting in excellent force retention, and 4) its output force increases sharply in the latter half stage of the actuator's shrinking or stretching, leading to explosive force similar to that of the human muscles. In addition, we can fabricate different actuators with various materials to achieve different superior performances to meet different requirements.

#### *Potential Applications*

Our actuators can be used for multiple purposes due to their excellent properties and performances. 1) They can work in air or underwater, driven by negative pressure fluid, air or liquid. 2) They are suitable for pushing or pulling heavy loads due to their large output force in a small range of strokes and two-way work mode. 3) On some occasions requiring high reliable clamping, our actuators can drive a robotic end effector to clamp a heavy object with high force retention. On the other hand, they can adapt well to the gradually increasing load on some occasions. 4) Our actuators can also work in situations where explosive force is required. 5) The folding structures make them adapt to some space-limited applications.



**FIG. 9.** Demonstration of the use of our actuators. (a) The carbon-fiber-beamed actuator with a 3D-printed skeleton pushing and (b) pulling a concrete block (8.1kg). (c) The actuator with a machined metal skeleton pulling a spring and (d) punching a pencil to break. (e) The actuator with a machined metal skeleton lifting rebar at total weight 60.5 kg. (f) Clamping a concrete block with a clamping gripper driven by the actuator with a machined skeleton. (g) The carbon-fiber-beamed actuator with a 3D printed skeleton assisting the movement of the model's arm. (h) The PET-beamed actuator with a 3D printed skeleton moving in water.

## Conclusions

Inspired by the cross-bridge structure in muscles, we propose a novel soft actuator concept and fabricate five prototypes with different materials. The performance test shows that our actuators driven by negative pressure fluid can simultaneously output large force and achieve high force retention. Also, it can either stretch or shrink and produce human-muscle-like explosive force. The five actuators' performances vary. The actuator with a machined skeleton can reach a full pull force of 1125.9N and a maximum thrust force of 818.2N. The actuator with a patched skeleton can output the maximal force 600 times its weight. As demonstrated, our actuators have vast potential for applications where stretching, shrinking, clamping, power assistance, and underwater movement are involved. Our ongoing work is to further design an actuator with an offset structure for bending motion based on this flexible actuator.

## Author Disclosure Statement

No competing financial interests exist.

## Funding Information

This work was supported in part by the National Key R&D Program of China (Grant No. 2021YFF0500900), National Natural Science Foundation of China (Grant No. 61773115), and Shenzhen Fundamental Research Program (Grant No. CYJ20190813152401690).

## Supplementary Material

Supplementary Movie S1  
 Supplementary Movie S2  
 Supplementary Movie S3  
 Supplementary Movie S4  
 Supplementary Movie S5  
 Supplementary Movie S6  
 Supplementary Movie S7  
 Supplementary Movie S8

## References

- Mazzolai B, Margheri L, Cianchetti M, Dario P, Laschi C. Soft-Robotic Arm Inspired by the Octopus: II. from Artificial Requirements to Innovative Technological Solutions. *Bioinspiration and Biomimetics*. 2012;7(2).
- Cianchetti M, Calisti M, Margheri L, Kuba M, Laschi C. Bioinspired Locomotion and Grasping in Water: The Soft Eight-Arm OCTOPUS Robot. *Bioinspiration and Biomimetics*. 2015;10(3).
- Yin H, Tian L, Yang G. Design of Fibre Array Muscle for Soft Finger with Variable Stiffness Based on Nylon and Shape Memory Alloy. *Adv. Robot*. 2020;34(9):599–609.
- Huang X, Ford M, Patterson ZJ, Zarepoor M, Pan C, Majidi C. Shape Memory Materials for Electrically-Powered Soft Machines. *J. Mater. Chem. B*. 2020;8(21):4539–4551.
- Moss A, Krieg M, Mohseni K. Modeling and Characterizing a Fiber-Reinforced Dielectric Elastomer Tension Actuator. *IEEE Robot. Autom. Lett*. 2021;6(2):1264–1271.
- Li WB, Zhang WM, Zou HX, Peng ZK, Meng G. A Fast Rolling Soft Robot Driven by Dielectric Elastomer. *IEEE/ASME Trans. Mechatronics*. 2018;23(4):1630–1640.
- Liang W, Liu H, Wang K, Qian Z, Ren L, Ren L. Comparative Study of Robotic Artificial Actuators and Biological Muscle. *Adv. Mech. Eng*. 2020;12(6):1–25.
- Wang H, Chen J, Lau HYK, Ren H. Motion Planning Based on Learning from Demonstration for Multiple-Segment Flexible Soft Robots Actuated by Electroactive Polymers. *IEEE Robot. Autom. Lett*. 2016;1(1):391–398.
- Ishiki A, Nabae H, Kodaira A, Suzumori K. PF-IPMC: Paper/Fabric Assisted IPMC Actuators for 3D Crafts. *IEEE Robot. Autom. Lett*. 2020;5(3):4035–4041.
- Yi X, Chakarvarthy A, Chen Z. Cooperative Collision Avoidance Control of Servo/IPMC Driven Robotic Fish with Back-Relaxation Effect. *IEEE Robot. Autom. Lett*. 2021;6(2):1816–1823.
- Zhu Z, Bian C, Ru J, Bai W, Chen H. Rapid Deformation of IPMC under a High Electrical Pulse Stimulus Inspired by Action Potential. *Smart Mater. Struct*. 2019;28(1).
- Hao Y, Gong Z, Xie Z, Guan S, Yang X, Wang T, Wen L. A Soft Bionic Gripper with Variable Effective Length. *J. Bionic Eng*. 2018;15(2):220–235.
- Yan J, Xu Z, Shi P, Zhao J. A Human-Inspired Soft Finger with Dual-Mode Morphing Enabled by Variable Stiffness Mechanism. *Soft Robot*. 2021;00(00).
- Sparman B, du Pasquier C, Thomsen C, Darbari S, Rustom R, Laucks J, Shea K, Tibbits S. Printed Silicone Pneumatic Actuators for Soft Robotics. *Addit. Manuf*. 2021;40(January):101860.
- Chen G, Yang X, Zhang X, Hu H. Water Hydraulic Soft Actuators for Underwater Autonomous Robotic Systems. *Appl. Ocean Res*. 2021;109(December 2020):102551.
- Bell MA, Gorissen B, Bertoldi K, Weaver JC, Wood RJ. A Modular and Self-Contained Fluidic Engine for Soft Actuators. *Adv. Intell. Syst*. 2021;21000942100094.
- Wang B, Guo W, Feng S, Hongdong Y, Wan F, Song C. Volumetrically Enhanced Soft Actuator with Proprioceptive Sensing\*. *IEEE Robot. Autom. Lett*. 2021;6(3):5284–5291.
- Ke X, Jang J, Chai Z, Yong H, Zhu J, Chen H, Guo CF, Ding H, Wu Z. Stiffness Preprogrammable Soft Bending Pneumatic Actuators for High-Efficient, Conformal Operation. *Soft Robot*. 2021;00(00):1–12.
- Wirekoh J, Park Y. Design of Flat Pneumatic Artificial Muscles. *Smart Mater. Struct*. 2017.

20. Wirekoh J, Valle L, Pol N, Park YL. Sensorized, Flat, Pneumatic Artificial Muscle Embedded with Biomimetic Microfluidic Sensors for Proprioceptive Feedback. *Soft Robot.* 2019;6(6):768–777.
21. Hu L, Gau D, Nixon J, Klein M, Fan Y, Menary G, Roche ET. Precurved, Fiber-Reinforced Actuators Enable Pneumatically Efficient Replication of Complex Biological Motions. *Soft Robot.* 2021;00(00):1–16.
22. Yang HD, Greczek BT, Asbeck AT. Modeling and Analysis of a High-Displacement Pneumatic Artificial Muscle with Integrated Sensing. *Front. Robot. AI.* 2019;6(JAN):1–13.
23. Shaheen R, Doumit M, Helal A. Design and Characterization of a Hyperelastic Tubular Soft Composite. *J. Mech. Behav. Biomed. Mater.* 2017;75(July):228–235.
24. Al-Fahaam H, Davis S, Nefti-Meziani S. The Design and Mathematical Modelling of Novel Extensor Bending Pneumatic Artificial Muscles (EBPAMs) for Soft Exoskeletons. *Rob. Auton. Syst.* 2018; 99:63–74.
25. Guan Q, Sun J, Liu Y, Wereley NM, Leng J. Novel Bending and Helical Extensile/Contractile Pneumatic Artificial Muscles Inspired by Elephant Trunk. *Soft Robot.* 2020;00(00):1–18.
26. Zhu M, Do TN, Hawkes E, Visell Y. Fluidic Fabric Muscle Sheets for Wearable and Soft Robotics. *Soft Robot.* 2020;7(2):179–197.
27. Kim W, Park H, Kim J. Compact Flat Fabric Pneumatic Artificial Muscle (FfPAM) for Soft Wearable Robotic Devices. *IEEE Robot. Autom. Lett.* 2021;6(2):2603–2610.
28. Naclerio ND, Hawkes EW. Simple, Low-Hysteresis, Folding, Fabric Pneumatic Artificial Muscle. *IEEE Robot. Autom. Lett.* 2020;5(2):3406–3413.
29. Kulasekera AL, Arumathanthri RB, Chathuranga DS, Gopura RARC, Lalitharatne TD. A Thin-Walled Vacuum Actuator (ThinVAc) and the Development of Multi-Filament Actuators for Soft Robotic Applications. *Sensors Actuators A Phys.* 2021;332113088.
30. Yu B, Yang J, Du R, Zhong Y. A Versatile Pneumatic Actuator Based on Scissor Mechanisms: Design, Modeling, and Experiments. *IEEE Robot. Autom. Lett.* 2021;6(2):1288–1295.
31. Li S, Vogt DM, Rus D, Wood RJ. Fluid-Driven Origami-Inspired Artificial Muscles. *Proc. Natl. Acad. Sci. U. S. A.* 2017;114(50):13132–13137.
32. Li S, Vogt DM, Bartlett NW, Rus D, Wood RJ. Tension Pistons: Amplifying Piston Force Using Fluid-Induced Tension in Flexible Materials. *Adv. Funct. Mater.* 2019;29(30):1–9.
33. Lee JG, Rodrigue H. Origami-Based Vacuum Pneumatic Artificial Muscles with Large Contraction Ratios. *Soft Robot.* 2019;6(1):109–117.
34. Liu T, Xia H, Lee DY, Firouzeh A, Park YL, Cho KJ. A Positive Pressure Jamming Based Variable Stiffness Structure and Its Application on Wearable Robots. *IEEE Robot. Autom. Lett.* 2021;6(4):8078–8085.
35. Ranzani T, Gerboni G, Cianchetti M, Menciassi A. A Bioinspired Soft Manipulator for Minimally Invasive Surgery. *Bioinspiration and Biomimetics.* 2015;10(3).
36. Ranzani T, Cianchetti M, Gerboni G, Falco I De, Menciassi A. A Soft Modular Manipulator for Minimally Invasive Surgery: Design and Characterization of a Single Module. *IEEE Trans. Robot.* 2016;32(1):187–200.
37. De Falco I, Cianchetti M, Menciassi A. A Soft Multi-Module Manipulator with Variable Stiffness for Minimally Invasive Surgery. *Bioinspiration and Biomimetics.* 2017;12(5).
38. Li Y, Chen Y, Yang Y, Wei Y. Passive Particle Jamming and Its Stiffening of Soft Robotic Grippers. *IEEE Trans. Robot.* 2017;33(2):446–455.
39. Yan J, Shi P, Xu Z, Zhao J. A Wide-Range Stiffness-Tunable Soft Actuator Inspired by Deep-Sea Glass Sponges. *Soft Robot.* 2021;00(00):1–13.
40. Wang Y, Yang Z, Zhou H, Zhao C, Barimah B, Li B, Xiang C, Li L, Gou X, Luo M. Inflatable Particle-Jammed Robotic Gripper Based on Integration of Positive Pressure and Partial Filling. *Soft Robot.* 2021;00(00):1–15.
41. Frontera W R , Ochala J . Skeletal Muscle: A Brief Review of Structure and Function[J]. *Calcified Tissue International,* 2015, 96(3):183-195.
42. Tillin N A , Pain M T G , Folland J P . Contraction speed and type influences rapid utilisation of available muscle force: neural and contractile mechanisms[J]. *Journal of Experimental Biology,* 2018, 221(24):jeb.193367.
43. Vecchio A D , Negro F , Holobar A , et al. You are as fast as your motor neurons: speed of recruitment and maximal discharge of motor neurons determine the maximal rate of force development in humans[J]. *The Journal of Physiology,* 2019, 597(9).
44. Mukund K , Subramaniam S . Skeletal muscle: A review of molecular structure and function, in health and disease[J]. *Wiley Interdisciplinary Reviews: Systems Biology and Medicine,* 2020, 12(1).

Adress corresponding to:

Jun Li

Ministry of Education Key Laboratory of Measurement and Control of CSE

Southeast University  
Nanjing 210096  
China

E-mail: [j.li@seu.edu.cn](mailto:j.li@seu.edu.cn)